S-1 Plots of Symmetric Molecule Generators
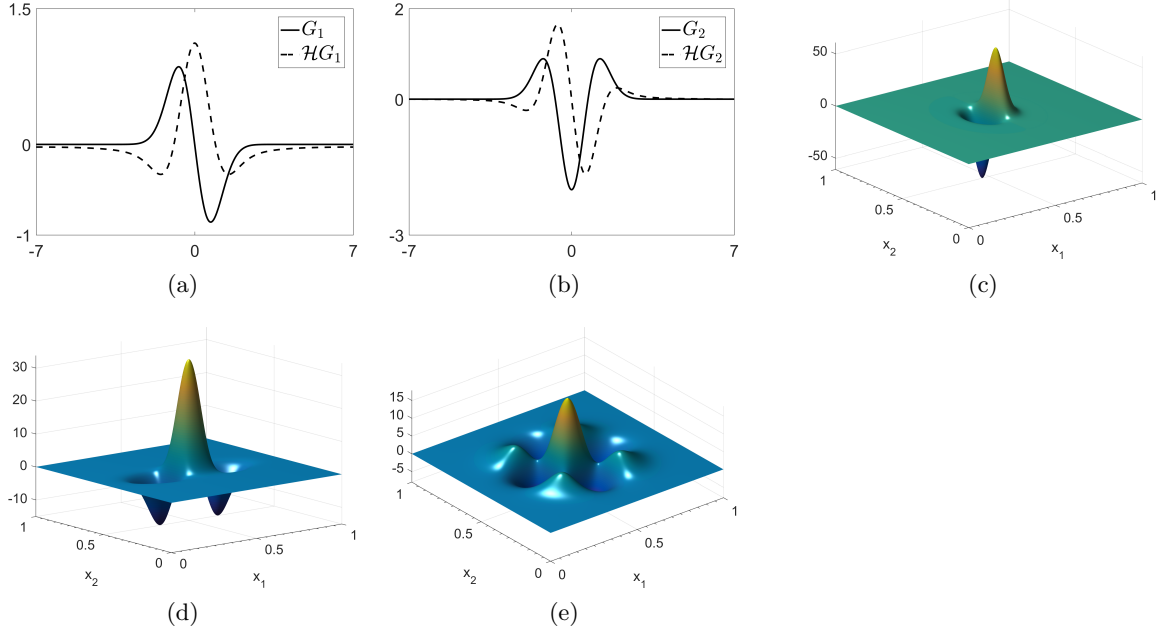
Figure S-1: Examples for L^1-normalized one- and two-dimensional symmetric generators. (a): First derivative of the Gaussian G_1 plotted together with its Hilbert transform $\mathcal{H}G_1$. (b): The second derivative of the Gaussian and its Hilbert transform. (c): Odd-symmetric 2D generator given by a separable product of G_1 and G_0. (d): Even-symmetric 2D generator based on G_2 and G_0. (e): Even-symmetric 2D generator given by the tensor product of G_2 with itself.

S-2 Implementation for Digital Images

A MATLAB toolbox named *Symmetric Molecule-based Feature Detector* (SymFD) that implements the measures defined in Section 3 for digital two-dimensional grayscale images can be downloaded from `http://www.math.uni-bremen.de/cda/software.html`. SymFD uses cyclic two-dimensional convolutions with digital symmetric molecule filters to obtain the required even- and odd-symmetric coefficients. The convolutions are carried out in the frequency domain via the fast Fourier transform (FFT). The computational complexity of the evaluation of any of the measures implemented in SymFD is thus of order $O(MN\log(N))$, where N denotes the number of pixels of the input image and M the number of considered symmetric molecule filters.

A main difficulty of developing digital implementations of the proposed feature detectors is to find a parametrization that makes it easy to configure SymFD for different types of applications and inputs while retaining the flexibility of the original definitions. In this section, we briefly summarize how systems of digital symmetric molecule filters can be defined and how the different parameters of the proposed edge, ridge, and blob measures are represented in SymFD.

1
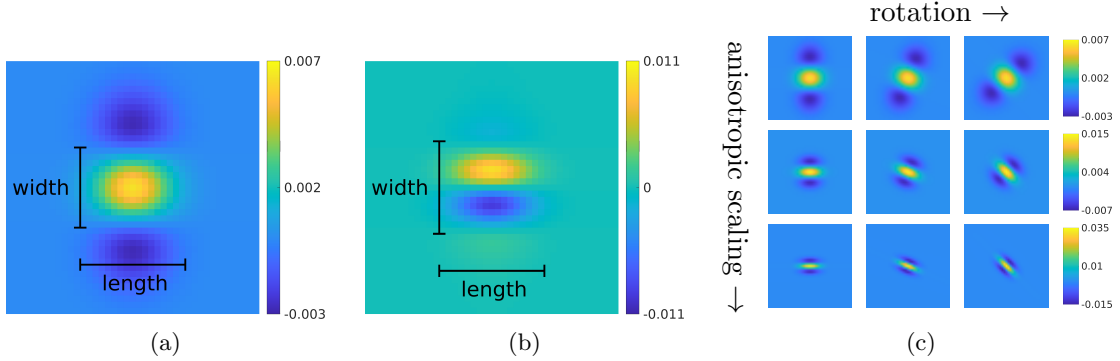
Figure S-2: (a): Example of an even-symmetric molecule filter. (b): Example of an odd-symmetric molecule filter. (c): Digital symmetric molecule filters that were obtained by rotating and anisotropically dilating the even-symmetric generator depicted in (a) ($\alpha = 0.2$).

In the continuum, a symmetric molecule system $SM(g, \alpha, a, J, \Theta) \subset L^1 \cap L^2(\mathbb{R}^2)$ is defined by an even- or odd-symmetric generator $g \in L^1 \cap L^2(\mathbb{R}^2)$, an anisotropy parameter $\alpha \in [0, 1]$, a constant scaling factor $a > 0$, a set of scaling parameters $J \subset \mathbb{Z}$, and a set of rotation parameters $\Theta \subset \mathbb{T}$ (see (28)). In SymFD, digital symmetric molecule filters are constructed by sampling the frequency domain representations $\widehat{m_{j,\theta,y}}(\xi)$ of symmetric molecules on a uniformly spaced grid of the size of the given input image. Note that all even- and odd-symmetric generators in the set $\Psi_2^{\mathrm{e}} \cup \widetilde{\Psi_2^{\mathrm{e}}} \cup \Psi_2^{\mathrm{o}}$ are based on tensor products of derivatives of the one-dimensional Gaussian and their Hilbert transforms (see Equations (25) to (27)), for which we can use the explicit formulations in the Fourier domain (9) and (10). Each function in the set $\Psi_2^{\mathrm{e}} \cup \widetilde{\Psi_2^{\mathrm{e}}} \cup \Psi_2^{\mathrm{o}}$ of two-dimensional symmetric generators is associated with two scaling parameters $c_1, c_2 \in \mathbb{R}_{>0}$ that determine the shape of their effective support (cf. (28)). In SymFD, the parameters `maxFeatureWidth` and `maxFeatureLength` can be used to directly specify the width and length of a generating symmetric molecule filter in terms of pixels. Here, the width is defined as the distance between the two zero crossings of the associated one-dimensional wavelet that are closest to the origin while the length is defined as the size of the interval centered on the origin which contains 95 % of the energy of the dilated one-dimensional Gaussian. Figures S-2a and S-2b depict examples of an even-symmetric and an odd-symmetric digital filter, respectively, and their corresponding lengths and widths. Note that in the case of even-symmetric molecules, this notion of width agrees with the definition of the radius given in Equations (49) and (58).

The anisotropy parameter α is equivalent to the parameter `alpha` in SymFD. The constant scaling factor a is parameterized by the value `scalesPerOctave` which determines the number of scales within each dyadic scaling step, that is,

$$a = 2^{1/\texttt{scalesPerOctave}}. \tag{S-1}$$

The set of scaling parameters J can then be specified via the parameter `minFeatureWidth` which defines the width of the symmetric molecule filters on the scale associated with the highest frequencies. That is, $J = \{0, \ldots, j_{\max}\}$ with

$$j_{\max} = \max\left\{ j \in \mathbb{N} \colon a^{-j}\texttt{maxFeatureWidth} \geq \texttt{minFeatureWidth} \right\}. \tag{S-2}$$

In SymFD, the set of rotation parameters Θ is defined by the integer `nOrientations` as a

sequence of uniformly spaced samples from the interval $[-\frac{\pi}{2}, \frac{\pi}{2})$, that is,

$$\Theta = \left\{ \theta_n = \frac{n\pi}{\texttt{nOrientations}} - \frac{\pi}{2} \right\}_{n=0}^{\texttt{nOrientations}-1}. \tag{S-3}$$

Examples of differently dilated and rotated digital symmetric molecule filters are plotted in Figure S-2c. SymFD furthermore supports the use of both rotation matrices R_θ (see (2)) and shear matrices

$$S_s = \begin{pmatrix} 1 & s \\ 0 & 1 \end{pmatrix}, \quad \text{and} \quad S_s^\mathsf{T} = \begin{pmatrix} 1 & 0 \\ s & 1 \end{pmatrix}, \quad s \in \mathbb{R}, \tag{S-4}$$

to change to preferred orientation of a symmetric generator. In practice, however, we recommend that one applies the rotation matrix R_θ. A main advantage of the shear operator is that it preserves the integer grid for shear parameters $s \in \mathbb{Z}$. This facilitates the construction of discrete shearlet transforms that provide a faithful transition between the continuous and the digital realm (e.g., [5, 9]). However, such transforms are typically only defined for special combinations of generators, scaling parameters, and orientation parameters and thus substantially lacking in flexibility. For this reason, all digital filters used in SymFD are constructed by sampling their analogs from the continuum in the Fourier domain. This approach yields maximal freedom but also renders the most significant advantage of applying shears instead of rotations moot.

Table S-1: Algorithms Evaluated in Section 4
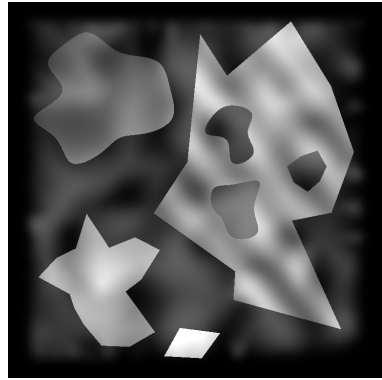
	Edges	Ridges	Blobs	Tangent Dir.	Widths	Parameters	Avg. Time
SymFD	✓	✓	✓	✓	✓	12	18.56 s
Shearlet [12]	✓	✗	✗	✓	✗	2	2.51 s
PhaseCong [8]	✓	✓	✗	✓	✗	11	1.53 s
Canny [3]	✓	✗	✗	✗	✗	3	0.39 s
Sobel [10]	✓	✗	✗	✗	✗	1	0.05 s
Steger [11]	✗	✓	✗	✗	✓	4	1.64 s
Frangi [6]	✗	✓	✗	✓	✗	8	0.43 s
Circular Hough [2, 4]	✗	✗	✓	✗	✓	4	0.36 s

The parameters introduced so far fully define a system of symmetric molecule filters that is based on a generator g which matches the symmetry of the feature that is to be detected (i.e., even symmetry in the cases of ridges and blobs and odd symmetry in the case of edges). In SymFD, the generator of opposite symmetry is by default constructed by applying the Hilbert transform to the one-dimensional wavelet used in the definition of g. Furthermore, a parameter `evenOddScaleOffset` can be used to define j^{e} in (44) and j^{o} in Equations (55) and (64).
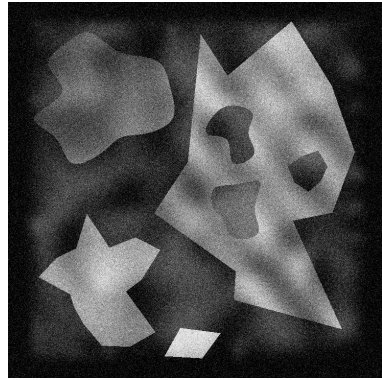
The soft-thresholding parameter β used in all three proposed feature measures is equivalent to the parameter `minContrast` in SymFD. Furthermore, SymFD implements two steps of post-processing that can be applied if necessary. The parameter `thinningThreshold` defines a threshold that is used to obtain a binary feature map which is then further processed with morphological thinning using MATLAB's `bwmorph` function. The parameter `minComponentLength` can be used to remove all connected components in the thinned binary feature map that do not have the specified minimal size.

Note that there also exists a Python implementation developed by Jonas Wloka, which is based on a previous version of the SymFD toolbox called *Complex Shearlet-Based Edge and Ridge Measure* (CoShREM). Both toolboxes can also be downloaded from `http://www.math.uni-bremen.de/cda/software.html`.
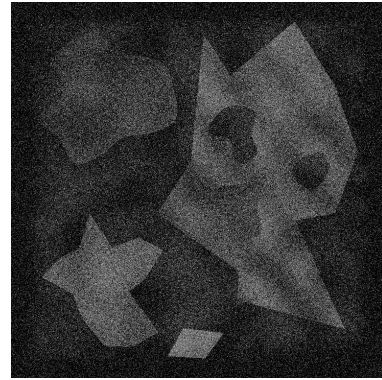
S-3   Supplemental Figures of Numerical Evaluation
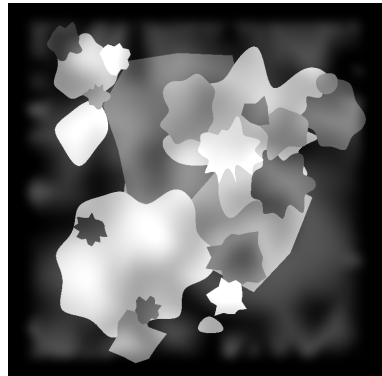
(a) *Synthetic image 1*   (b) Medium noise   (c) Severe noise
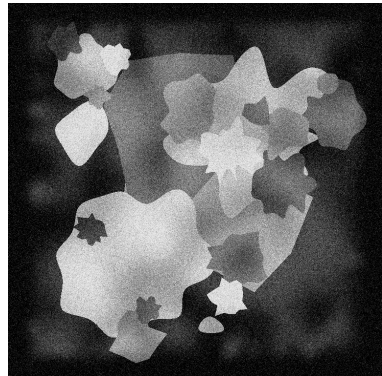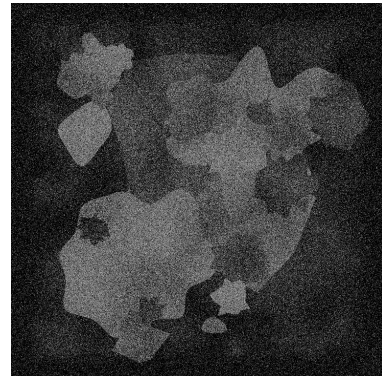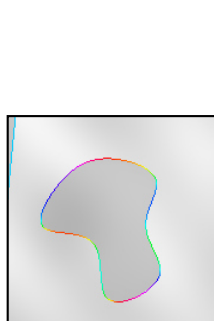
(d) *Synthetic image 2*   (e) Medium noise   (f) Severe noise
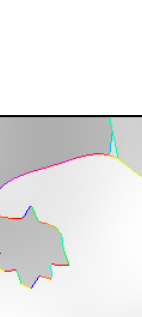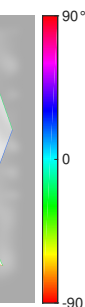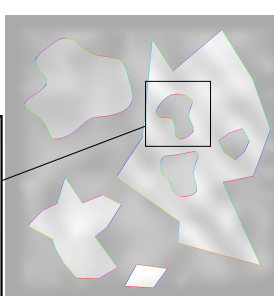
(g) Groundtruth for *synthetic image 1*   (h) Groundtruth for *synthetic image 2*
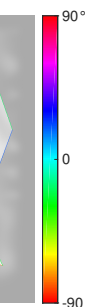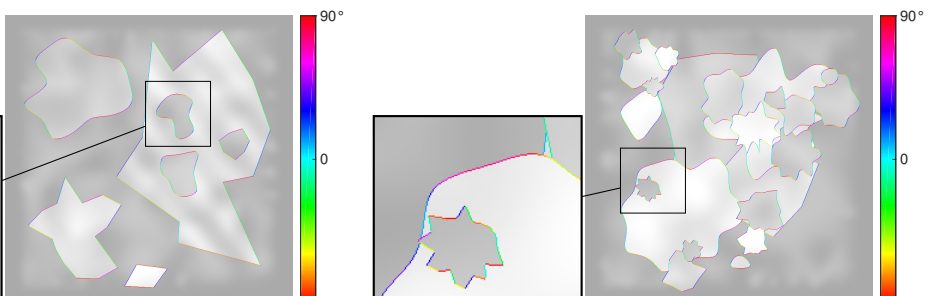
Figure S-3: The synthetic images and respective ground truths used for the evaluation of different edge detection methods.

(a) *Synthetic image 3*

(b) Medium noise

(c) Severe noise

(d) *Synthetic image 4*

(e) Medium noise

(f) Severe noise

(g) Groundtruth for *synthetic image 3*

(h) Groundtruth for *synthetic image 4*
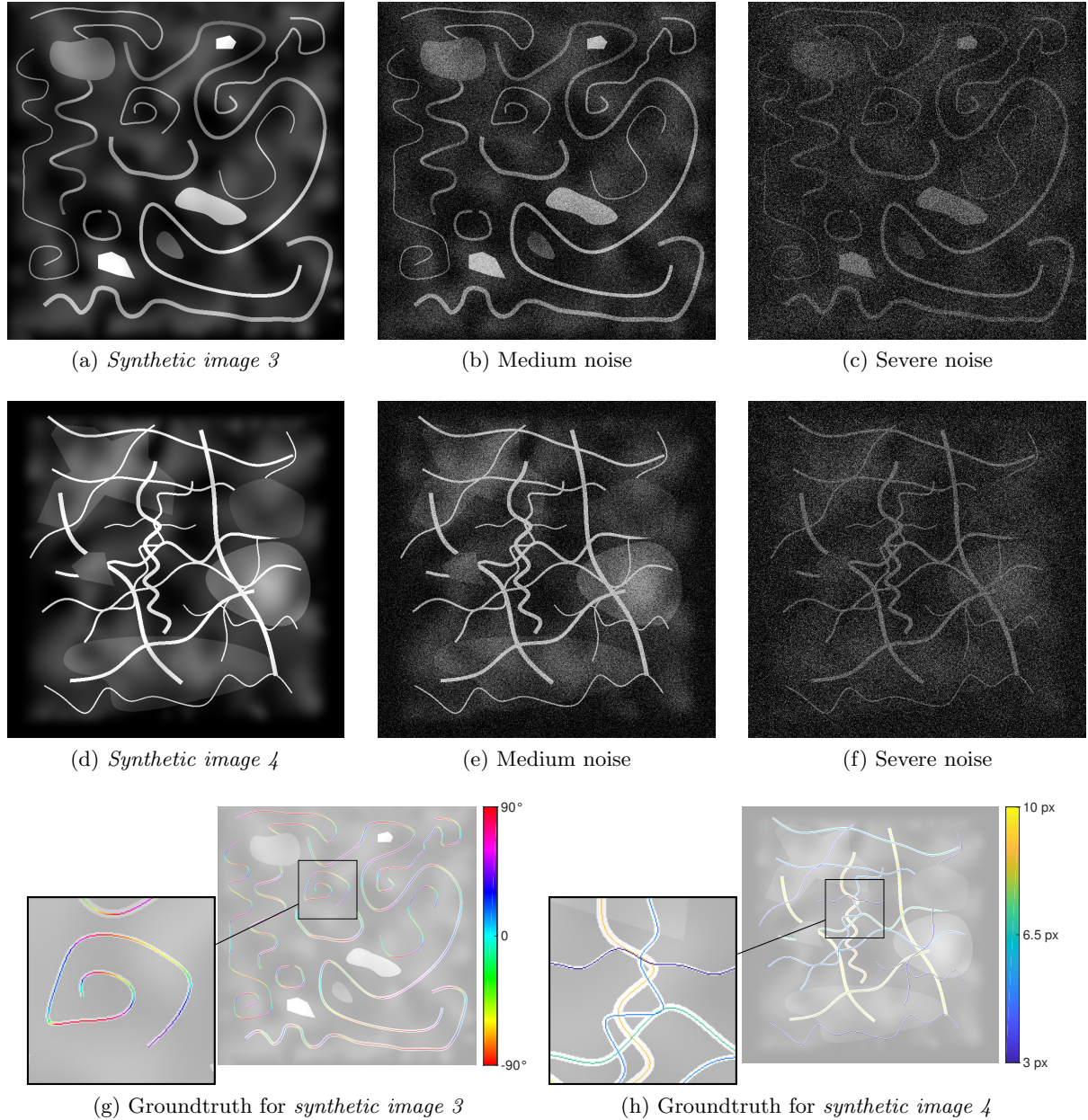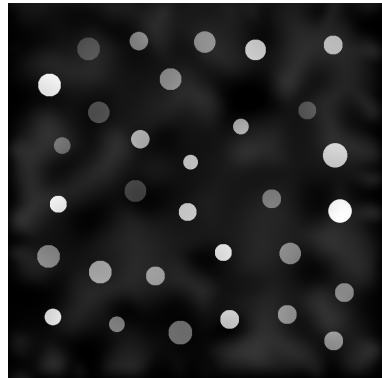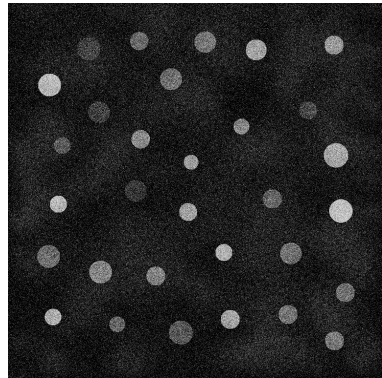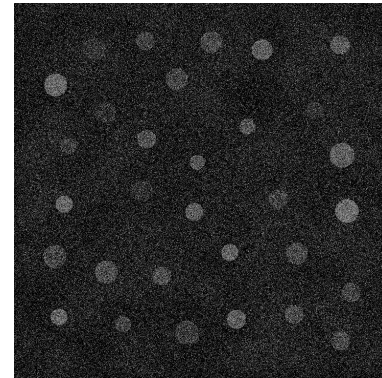
Figure S-4: The synthetic images and respective ground truths used for the evaluation of different ridge detection methods.
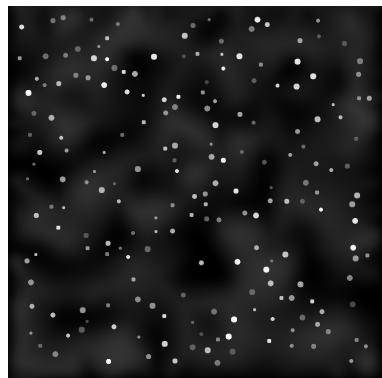
(a) *Synthetic image 5*　　　　　(b) Medium noise　　　　　(c) Severe noise
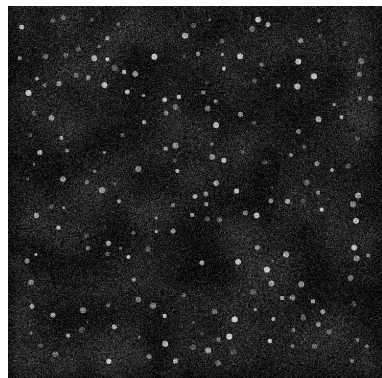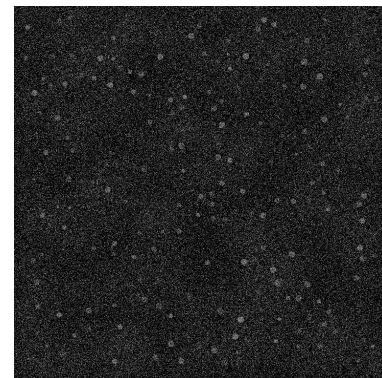
(d) *Synthetic image 6*　　　　　(e) Medium noise　　　　　(f) Severe noise
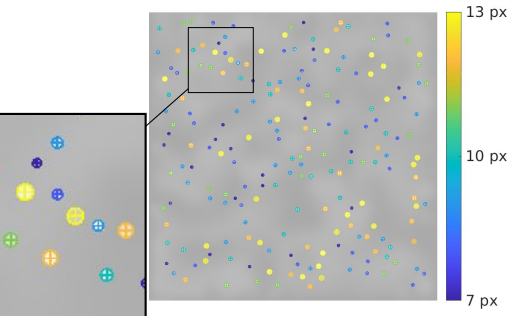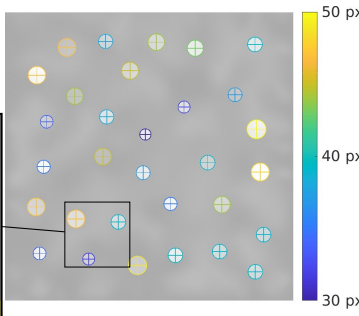
(g) Groundtruth for *synthetic image 5*　　　(h) Groundtruth for *synthetic image 6*

Figure S-5: The synthetic images and respective ground truths used for the evaluation of different blob detection methods.

(a) Input (*synthetic image 1*, medium noise)

(b) SymFD edge measure $\mathrm{E}(f, y)$

(c) Tangent directions $\mathrm{O_E}(f, y)$ after post-processing

(d) Error map for $\mathrm{O_E}(f, y)$
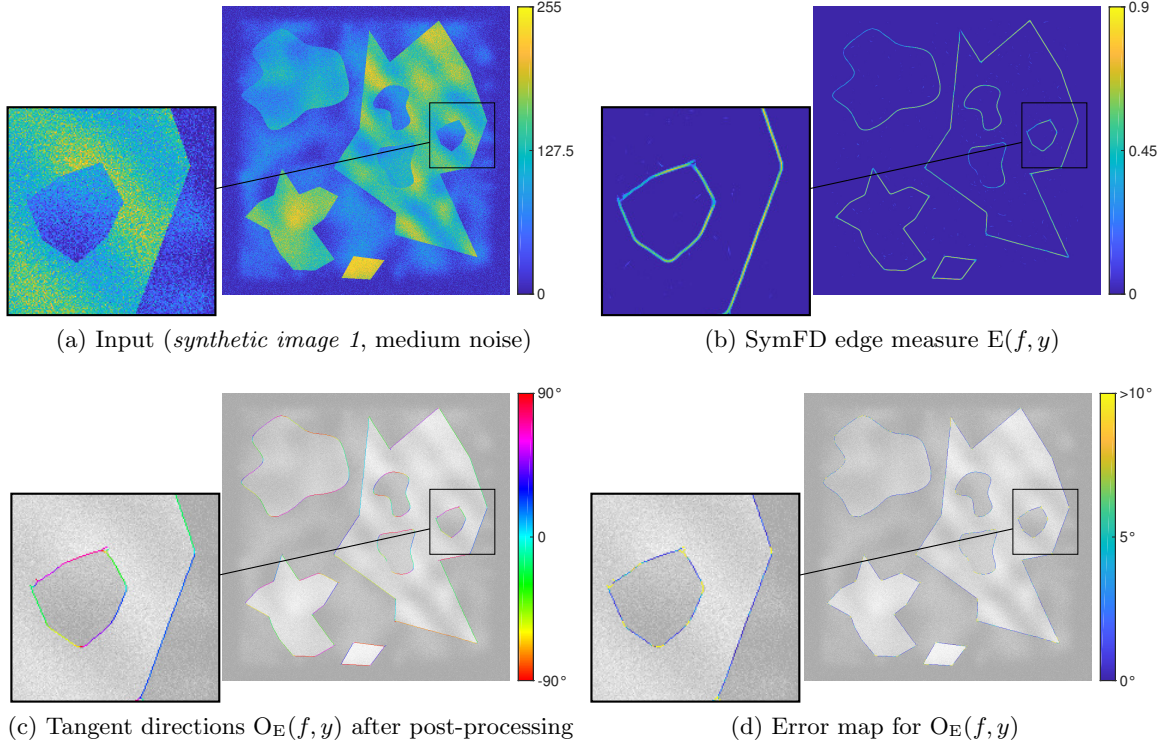
Figure S-6: Detection of edges and local tangent orientations in a synthetic image yielded by SymFD with parameters $\psi^{\mathrm{o}} = \frac{\mathcal{H}G_2}{\|\mathcal{H}G_2\|_{L^1}}$, $\psi^{\mathrm{e}} = \frac{G_2}{\|G_2\|_{L^1}}$, $\mathtt{maxFeatureWidth} = 16$, $\mathtt{maxFeatureLength} = 16$, $\alpha = \frac{1}{2}$, $\mathtt{minFeatureWidth} = 4$, $\mathtt{scalesPerOctave} = 2$, $\mathtt{nOrientations} = 16$, $j^{\mathrm{e}} = 1$, and $\beta = 15$. The input image is of size 768×768 and was distorted by a combination of Gaussian and Poisson noise.

(a) Input (*synthetic image 4*, severe noise)

(b) SymFD (tangent directions)

(c) SymFD (widths)

(d) Steger [11]

(e) Frangi [6]

(f) Phase congruency measure [8]
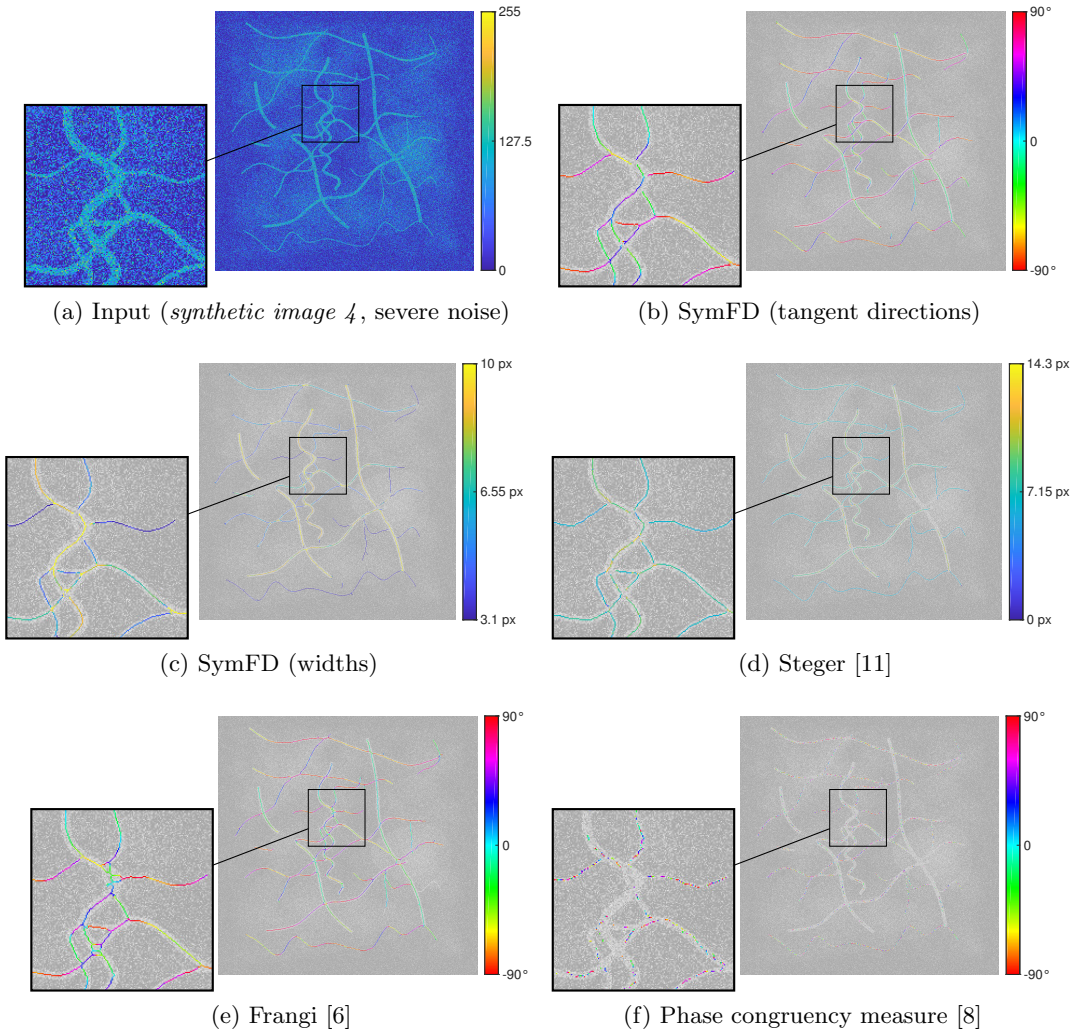
Figure S-7: Visual comparison of the detection results yielded by different ridge detection methods. Where applicable, the detected centerline of a ridge is shown in combination with estimates of the local tangent direction and/or the width of the ridge.

(a) Input (*synthetic image 6*, medium noise)

(b) SymFD blob measure $\mathrm{B}(f, y)$

(c) Widths $\mathrm{W_B}(f, y)$ after post-processing

(d) Error map for $\mathrm{W_B}(f, y)$
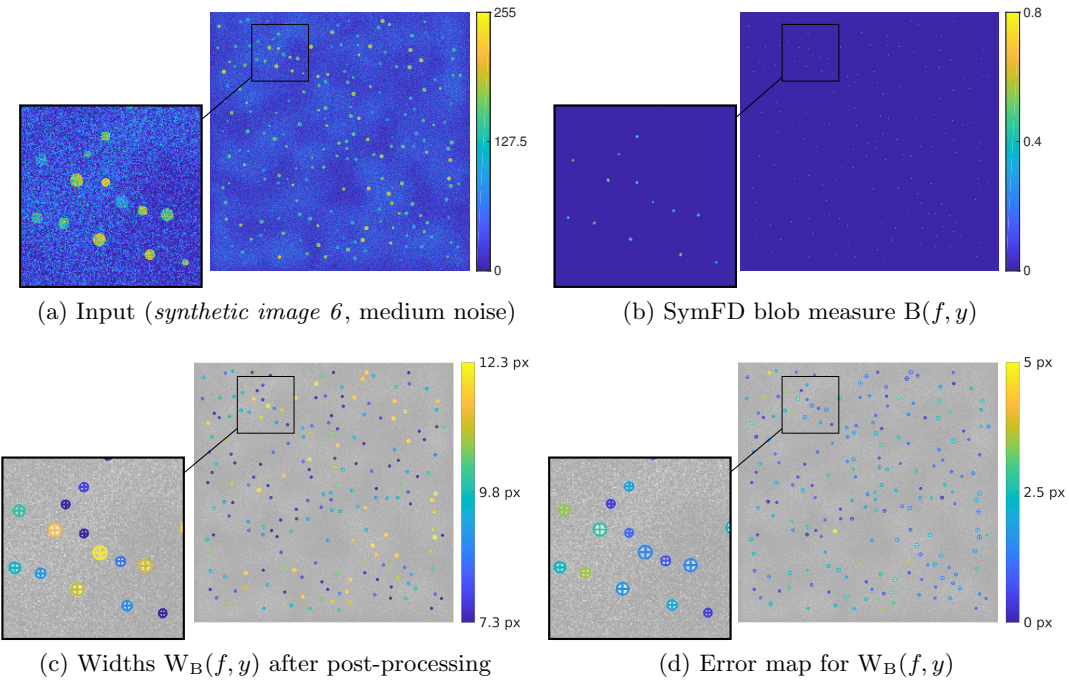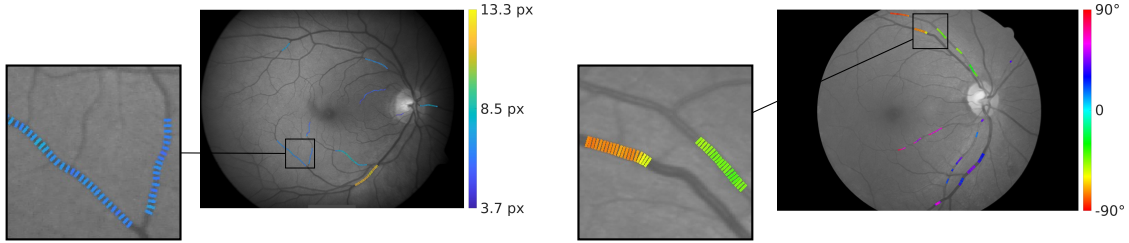
Figure S-8: Detection of blobs and blob widths (diameters) in a synthetic image. The results were yielded by SymFD with parameters $\psi^{\mathrm{e}} = \frac{\mathcal{H}G_1}{\|\mathcal{H}G_1\|_{L^1}}$, $\mathtt{maxFeatureWidth} = 16$, $\mathtt{maxFeatureLength} = 16$, $\alpha = 1$, $\mathtt{minFeatureWidth} = 6$, $\mathtt{scalesPerOctave} = 8$, $\mathtt{nOrientations} = 16$, $j^{\mathrm{o}} = 0$, and $\beta = 5$. All blobs in the input have positive contrast. The analysis is therefore restricted to locations y where the height measure is positive, i.e., $\mathrm{H_B}(f, y) \geq 0$. The input image is of size 768×768 and was distorted by a combination of Gaussian and Poisson noise.

(a) Image 7 of the REVIEW VDIS dataset with manually annotated vessel profiles.

(b) Image 2 of the REVIEW CLRIS dataset with manually annotated vessel profiles.

Figure S-9: Examples of digital images in the REVIEW retinal vessel reference dataset [1] with manually annotated ground truth vessel profiles.

(a) The shown image was acquired with a high-definition camera with a resolution of 1538×1536 pixels. Median human count of cell colonies: 1090.

(b) The shown image was obtained from a low-cost webcam with horizontal stripe artifacts and acquired at a resolution of 1000×1000 pixels. Median human count of cell colonies: 69.
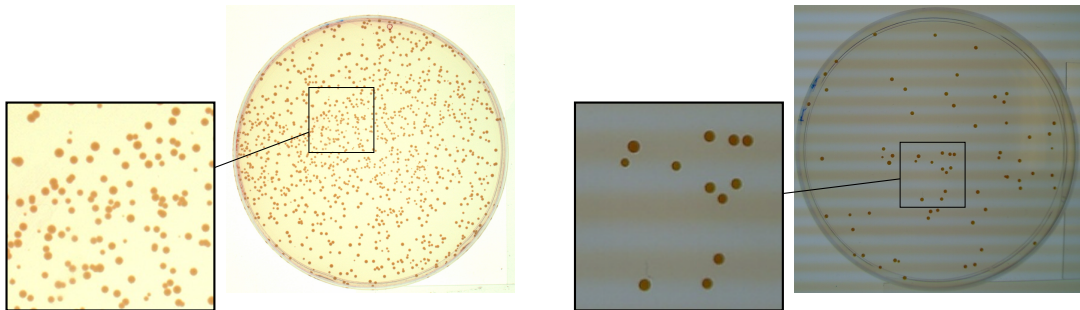
Figure S-10: Two pictures showing grown cell colonies in a Petri dish. The dataset containing the displayed images was originally developed for the evaluation of the OpenCFU software package [7].

References

[1] B. AL-DIRI, A. HUNTER, D. STEEL, M. HABIB, T. HUDAIB, AND S. BERRY, *REVIEW – a reference data set for retinal vessel profiles*, in 30th Annual International Conference of the IEEE Engineering in Medicine and Biology Society, Aug. 2008, pp. 2262–2265, `https://doi.org/10.1109/IEMBS.2008.4649647`.

[2] T. J. ATHERTON AND D. J. KERBYSON, *Size invariant circle detection*, Image Vis. Comput., 17 (1999), pp. 795–803.

[3] J. CANNY, *A computational approach to edge detection*, IEEE Trans. Pattern Anal. Mach. Intell., 8(6) (1986), pp. 679–698.

[4] E. DAVIES, *Chapter 10 – circle detection*, in Machine Vision, E. Davies, ed., Signal Processing and its Applications, Morgan Kaufmann, Burlington, third edition ed., 2005, pp. 283 – 313, `https://doi.org/https://doi.org/10.1016/B978-012206093-9/50013-7`.

[5] G. EASLEY, D. LABATE, AND W.-Q. LIM, *Sparse directional image representations using the discrete shearlet transform*, Appl. Comput. Harmon. Anal., 25 (2008), pp. 25 – 46, `https://doi.org/https://doi.org/10.1016/j.acha.2007.09.003`.

[6] A. F. FRANGI, W. J. NIESSEN, K. L. VINCKEN, AND M. A. VIERGEVER, *Multiscale vessel enhancement filtering*, in International Conference on Medical Image Computing and Computer-Assisted Intervention, Springer, 1998, pp. 130–137.

[7] Q. GEISSMANN, *OpenCFU, a new free and open-source software to count cell colonies and other circular objects*, PLos One, 8 (2013), pp. 1–10, `https://doi.org/10.1371/journal.pone.0054072`.

[8] P. KOVESI, *Image features from phase congruency*, Videre: A Journal of Computer Vision Research, 1(3) (1999), pp. 1–26.

[9] G. KUTYNIOK, W.-Q. LIM, AND R. REISENHOFER, *ShearLab 3D: faithful digital shearlet transforms based on compactly supported shearlets*, ACM Trans. Math. Software, 42 (2016), pp. 5:1–5:42, `https://doi.org/10.1145/2740960`.

[10] I. SOBEL AND G. FELDMAN, *A 3×3 isotropic gradient operator for image processing*. Presentation at the Stanford Artificial Intelligence Project, 1968.

[11] C. STEGER, *An unbiased detector of curvilinear structures*, IEEE Trans. Pattern Anal. Mach. Intell., 20 (1998), pp. 113–125.

[12] S. YI, D. LABATE, G. R. EASLEY, AND H. KRIM, *A shearlet approach to edge analysis and detection*, IEEE Trans. Image Process., 18 (2009), pp. 929–941, `https://doi.org/10.1109/TIP.2009.2013082`, `https://doi.org/10.1109/TIP.2009.2013082`.